Progress In Electromagnetics Research C, Vol. 134, 53–63, 2023

A Small-Scaled Super Wideband Circular Ring Fractal Antenna with High BDR for SHF Applications

Shobit Agarwal[1] and Umair Rafique[2, *]

Abstract—This paper presents a miniaturized super wideband (SWB) antenna that has a high bandwidth dimension ratio (BDR). It is intended for the use in microwave and millimeter-wave (mmWave) frequency applications. The designed antenna ensures low-dispersive behavior for both near- and far-field performance. The radiating element is composed of three circular rings that are interconnected by conical-shaped metal strips which lead to a fractal geometry. The design incorporates a partial ground plane and two parasitic patches located at the bottom and top sides of the substrate, respectively. The parasitic strips serve the purpose of enhancing impedance matching at lower frequency bands and reducing spurious radiation that may arise from the feed line. The proposed antenna has an overall size of $20 \times 20\,\text{mm}^2$ and exhibits an impedance bandwidth (IBW) of $\approx 57\,\text{GHz}$, spanning from 2.86 to beyond 60 GHz with a fractional bandwidth (FBW) of 181.8%, a ratio bandwidth (RBW) of 21 : 1, and a BDR of 5036. Furthermore, the peak gain value is observed to be $\approx 11\,\text{dBi}$, while the average gain within the operating range is $\approx 6\,\text{dBi}$. The proposed antenna design was also fabricated and tested, and experimental results show a reasonable agreement with the simulated data. This makes the antenna extremely suitable for energy harvesting applications in future fifth-generation (5G) and sixth-generation (6G) networks.

1. INTRODUCTION

In today's era, there is a significant demand for communication networks that offer high spectral efficiency and high data transfer speeds. Additionally, the ongoing advancements in wireless communication technologies are further contributing to this demand. To meet the aforementioned requirements, ultra-wideband (UWB) antennas are employed in several applications. As per the guidelines provided by the Federal Communication Commission (FCC), the operational bandwidth of planar UWB antennas lies in the frequency range of 3.1–10.6 GHz. These antennas are capable of facilitating short-range communications with great efficiency. In the current scenario, the antennas that can provide access to both short- and long-range communications are in demand. To meet this requirement, super wideband (SWB) antennas can be employed, which possess a ratio bandwidth (RBW) of at least 10 : 1. SWB antennas are compatible with high data rates and provide wide impedance bandwidth (IBW), increased channel range, and maximum resolution for wireless communication systems over UWB. No particular bandwidth criteria are defined for SWB antennas, as they could operate in any operating range; however, these antennas should necessarily maintain an RBW of at least 10 : 1 for a return loss of 10 dB. SWB antennas should also provide either directional or omnidirectional radiation characteristics, depending on the application. To accommodate the above-mentioned requirements, numerous SWB antennas have been reported in the literature.

Received 31 March 2023, Accepted 14 June 2023, Scheduled 28 June 2023
* Corresponding author: Umair Rafique (umair.rafique@ieee.org).
[1] Department of Electrical, Electronic and Information Technology, Università di Bologna, Bologna Campus, Italy. [2] Center for Wireless Communications, Faculty of Information Technology and Electrical Engineering, University of Oulu, Oulu 90570, Finland.

In [1], a co-planar waveguide (CPW)-fed planar elliptical antenna design was presented for SWB performance. A trapezoid-shaped ground plane with a tapered CPW feed was used for the design and achieved an RBW of 21.6 : 1. The same design technique was reported in [2] for a semi-elliptical patch radiator. In this case, the authors reported an RBW of 19.7 : 1. Despite having a high RBW, the above-presented designs can only marginally cover the UWB frequency spectrum. In [3], a novel patch radiator shape was used with a tapered feed line to achieve an extremely wide IBW. The same design technique was used by [4] and achieved an RBW of 34 : 1, which is higher than the design of [3]. In [5], the authors improved the IBW of the design presented in [1] by incorporating a semicircular branch with a feed line and radiator. By utilizing this technique, they achieved an IBW of $\approx$ 23 GHz in the frequency range of 1.02–24.1 GHz. They also reported another planar elliptical antenna in [6] for SWB applications. The same feeding technique was used as reported in [5] with a partial ground plane, and a bandwidth of 26.32 GHz (1.08 to 27.4 GHz) was observed. Chen et al. [7] designed a compact egg-shaped SWB planar monopole. With the use of a semi-elliptical fractal slot into an asymmetrical ground, they achieved a 172% FBW in the frequency range of 1.44–18.8 GHz. Gorai et al. [8] designed a CPW-fed propeller-shaped planar SWB antenna and achieved an RBW of 11.6 : 1 from 3 to 35 GHz. However, their design suffered due to a poor bandwidth dimension ratio (BDR), which was equal to 805.

Tang et al. [9] designed an elliptical slot antenna for SWB applications. The design was composed of an oval-shaped parasitic patch constructed in an elliptical slot and a microstrip-line-fed elliptical tuning fork. From the results, it was demonstrated that the antenna had a bandwidth of 19.92 GHz between 2.26 and 22.18 GHz. In [10], a transparent CPW-fed antenna was designed for enhanced IBW. A rectangular radiator with a staircase shape was employed along with two primary and two secondary rectangular symmetrical stubs on the ground plane to produce overlapping resonant frequencies. This configuration yields an IBW of 28.85 GHz between 3.15 and 32 GHz, a BDR of $\approx$ 1127, and an RBW of 10.16 : 1. In [11], a semi-circular planar antenna that was equipped with a trapezoid-shaped ground was investigated. The semi-circular patch was excited using a tapered microstrip feed line. The designed antenna provided a BDR of 4261 and an RBW of 15.38 : 1, along with an IBW ranging from 1.3 to 20 GHz. In [12], a miniaturized version of [6] was reported. With this design, the authors improved the lower operating frequency range and BDR. In [13], a planar antenna with a beveled-shaped radiator was presented for SWB communication. Two parasitic elements were designed on the upper side of the substrate, along with a tapered feed line, to improve the bandwidth. In [14], an elliptical fractal antenna was reported for SWB applications. The elliptical patch radiators are arranged in such a manner that the overall design looks like a tree, and a modified semi-elliptical ground was designed on the back side of the substrate. This design exhibits an IBW of 0.65 to 35.61 GHz and an RBW of 54.78 : 1.

In [15], a compact SWB antenna was designed with a combination of different geometries. The IBW was enhanced using a combination of square, circular, and trapezoidal slots on a rectangular radiator. The improvement in impedance matching at the lower frequencies was achieved by adding rectangular and trapezoidal slots in the ground plane. Through this configuration, the authors achieved a fractional bandwidth (FBW) of 185.41% in the operating bandwidth. In [16], a bulb-shaped CPW-fed planar SWB antenna was designed to achieve the FBW of 173.8% and BDR of 1904 from 2.8 to 40 GHz. In [17], a CPW-fed compact flower-shaped antenna was designed for SWB millimeter-wave (mmWave) applications. Through a combination of a flower-shaped radiator and an elliptical ground plane, a bandwidth of 3.7 to more than 60 GHz was achieved with an FBW of greater than 176.76% and a BDR of 2780.108. In [18], a slot antenna was presented for SWB applications. The IBW in the frequency range of 1.8–30 GHz was achieved by using a cardioid-like radiating structure and a slot. From the presented design, a BDR of 3062 and an FBW of 178% were achieved.

From the above-mentioned literature, it is observed that increasing the antenna's IBW either increases its overall size or deteriorates the BDR. Therefore, designing a compact antenna that has both SWB functionality and high BDR is a challenging task. Additionally, the antenna's configuration and geometry must be simple to allow for easy fabrication using low-cost production techniques such as chemical etching. As a solution, in this work, a small-scale, low-profile SWB antenna is proposed. The miniaturization is achieved by designing three annular rings and twelve conical-shaped strips together. For improved impedance matching, a partial ground plane with a stair-shaped slot is utilized at the bottom of the substrate, while two parasitic strips are utilized on top of the substrate to match the antenna impedance at lower frequency bands. From the presented configuration, a wide FBW of 181.8%

starting from 2.86 to 60 GHz is achieved with a fairly good BDR. As a further achievement, the antenna maintains almost constant behavior from both the radiation and the input impedance points of view in the whole operating range, thus earning a chance as the radiative part of future SWB rectifying antennas (rectennas).

The rest of the article is organized in the following way: The evolution of the proposed antenna is discussed in Section 2 followed by fabrication and testing in Section 3. The time-domain analysis of the antenna is discussed in Section 4. Finally, the conclusion drawn from the presented antenna design is given in Section 5.

2. PROPOSED FRACTAL ANTENNA DESIGN AND EVOLUTION

A schematic representation of the proposed fractal antenna is shown in Figure 1, while the final optimized dimensions are mentioned in Table 1. The top side of the antenna is composed of three annular rings of decreasing radius, and twelve conical-shaped strips, each having a cone angle of 7.7°, are placed uniformly around the center. The top surface of the antenna also comprises two metallic strips serving as parasitic elements. The partial ground plane with a stair-shaped slot is designed on the bottom side. The proposed antenna is designed on a Rogers RT-5880 having a dielectric constant (ε_r) of 2.2, a thickness (h) of 1.57 mm, and a loss tangent ($\tan\delta$) of 0.0009 @ 10 GHz (which varies between 0.0083 and 0.0009 within the operating frequency range). A 50 Ω microstrip feed line is used to excite the antenna designed using standard equations presented in [19].

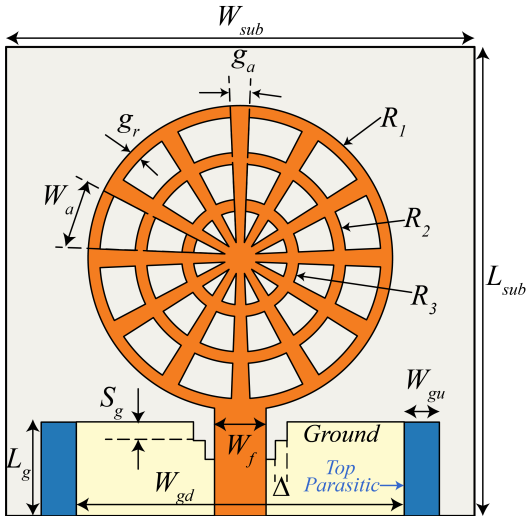

Figure 1. Schematic of the proposed SWB fractal antenna.

Table 1. Optimized dimensions of the proposed fractal antenna (values are in mm).

Parameter	Value	Parameter	Value
L_{sub}	20	R_1	6.5
W_{sub}	20	R_2	4.5
L_g	4	R_3	2.5
W_{gd}	14	W_a	22.3°
W_{gu}	1.5	g_a	7.7°
S_g	0.8	g_r	0.5
W_f	2.2	Δ	0.5

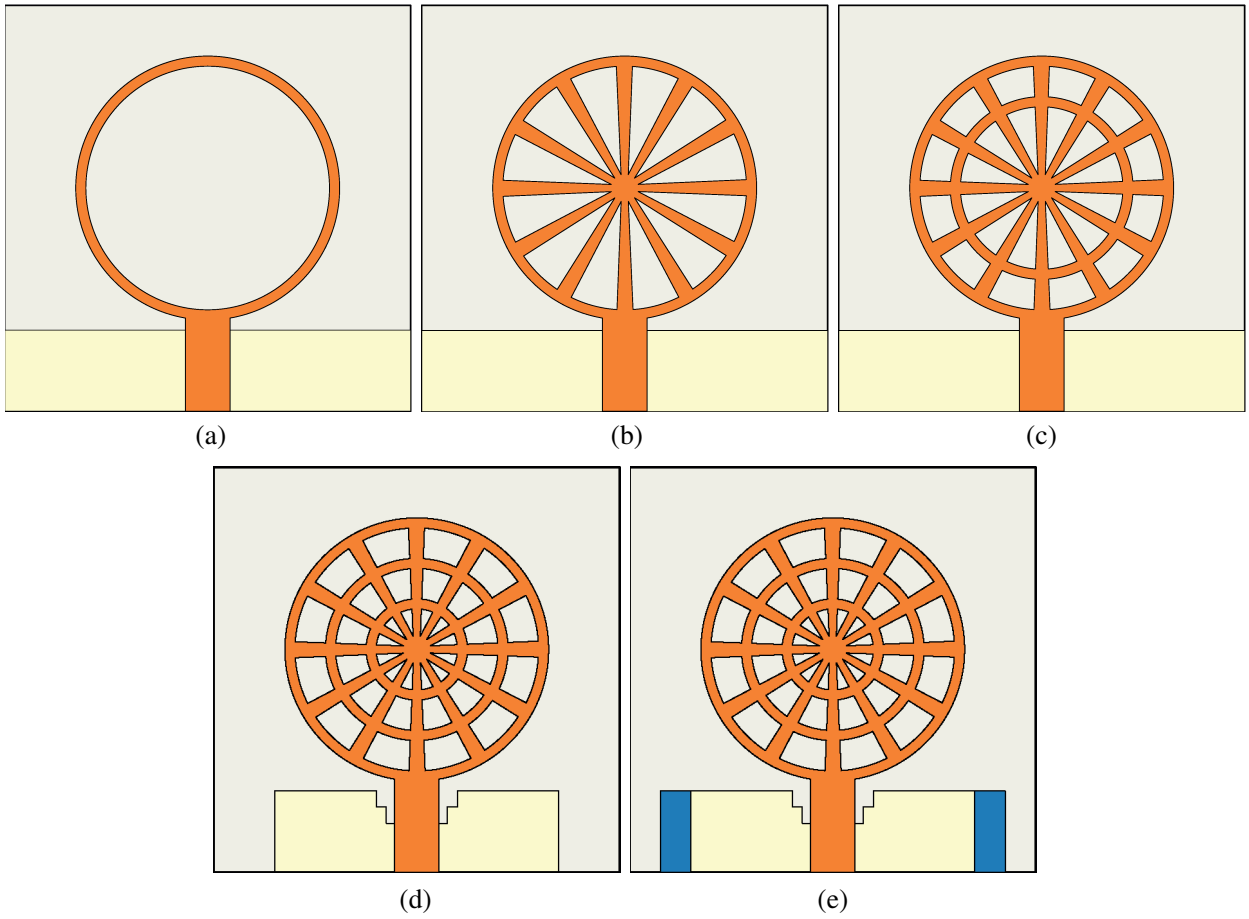

Figure 2. Evolution stages. (a) Iteration 1. (b) Iteration 2. (c) Iteration 3. (d) Iteration 4. (e) Proposed antenna.

All evolution stages for the proposed fractal antenna are shown in Figures 2(a)–(e). Referring to Figure 2(a), denoted as iteration 1, an annular ring radiator of radius R_1 is designed on the top side of the dielectric substrate, while a partial ground plane is placed on the bottom side. The outer radius of the annular ring is determined at 3 GHz using the analytical expressions presented in [20]. The partial ground plane is utilized to help achieve a wideband response, as commonly done for wideband monopole antennas. The simulated reflection coefficient (S_{11}) response of the iteration 1 design is shown in Figure 3(a).

From Figure 3(a) (brown curve), it is observed that iteration 1 design provides a multi-band response for frequency ranges 3.24–4.1 GHz, 16.4–18.12 GHz, 21.83–23.07 GHz, 27.8–37.2 GHz, and 45.7–60 GHz. To enhance the IBW, twelve conical-shaped metallic strips are added in the annular ring, and this modification is named as iteration 2, as shown in Figure 2(b). Each metallic strip contributes an angular width of 7.7°, while the non-metallic part has an angular width of 22.3°. Compared to iteration 1 design, this design performs better, especially for lower frequencies (see Figure 3(a), green curve), because the utilization of conical-shaped metallic strips allows current to pass through multiple paths (resulting in an increase in the overall electrical length), which generates multiple resonances at a lower frequency and improves the antenna performance. However, iteration 2 design also provides a multi-band response for different frequency ranges, i.e., 3.22–13.56 GHz, 16–17.5 GHz, 19.7–20.30 GHz, 22.54–24.3 GHz, 28.28–37.10 GHz, and 42.1–60 GHz, as shown in Figure 3(a) (green curve). To further improve the antenna's bandwidth performance in the middle frequency region, another annular ring of radius $R_2 < R_1$ is added in iteration 2 design, as shown in Figure 2(c) and is designated as iteration 3. Iteration 3 antenna design operates well for lower- and middle-frequency ranges (see Figure 3(a), purple

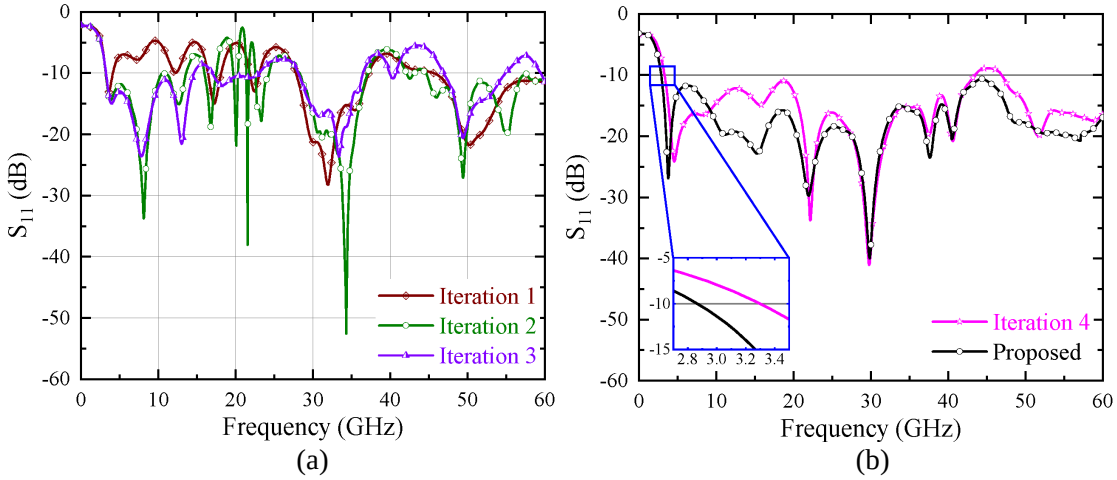

Figure 3. Simulated S_{11} response of all evolution stages.

curve); however, an impedance mismatch is observed at higher frequencies. To obtain SWB response and to improve matching in the higher frequency range, another annular ring of radius R_3 (smaller than R_2 and R_1) is added to iteration 3 design, and a slot of stair-shape is introduced in the ground plane, as shown in Figure 2(d). The incorporation of a slot in the ground plane and the addition of a third annular ring offered improved impedance matching in the operating frequency range, as shown in Figure 3(b) (pink curve). Finally, for improved matching at lower frequency bands, two parasitic strips are placed on the top side of the substrate, as shown in Figure 2(e). These parasitic strips minimize the effect of spurious radiation caused by the feed line [13, 21, 22] and ultimately lead to enhanced IBW. This modification tends to achieve SWB response from 2.86 to more than 60 GHz, as shown in Figure 3(b) (black curve).

To gain further insight about the antenna operation, the surface current density at four different frequencies, i.e., 5 GHz, 20 GHz, 35 GHz, and 55 GHz, is shown in Figure 4. From the figure, it is evident that the outermost circle is responsible for the resonances at lower frequencies, as shown in Figure 4(a). As the frequency increases, the inner circles start contributing and generating resonances at higher frequencies, as illustrated in Figures 4(b)–(d). This behavior is also in accordance with the conventional antenna theory [19].

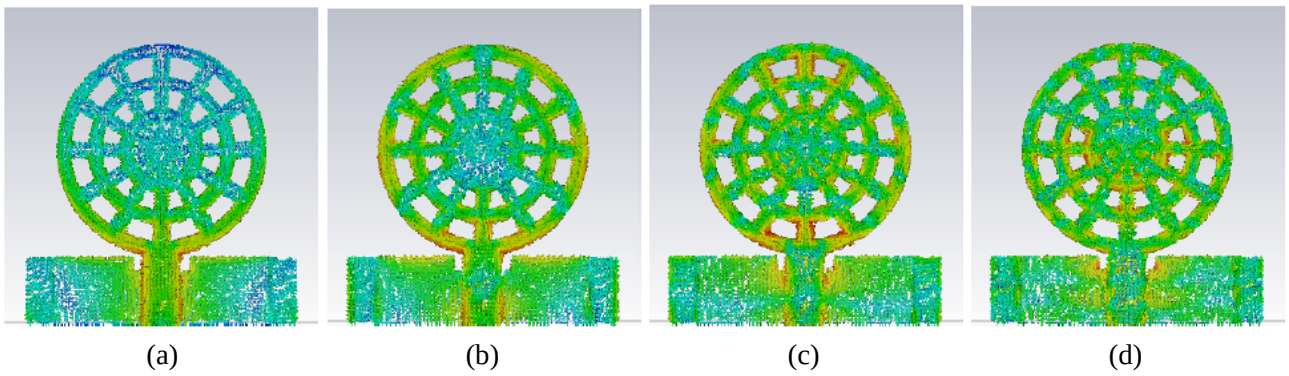

Figure 4. Surface current density at (a) 5 GHz, (b) 20 GHz, (c) 35 GHz, (d) 55 GHz.

3. FABRICATION AND VALIDATION

To verify the simulated data, a prototype of the designed fractal antenna is fabricated (shown in the inset of Figure 5) using a low-cost photolithography technique and measured using the Agilent Technologies

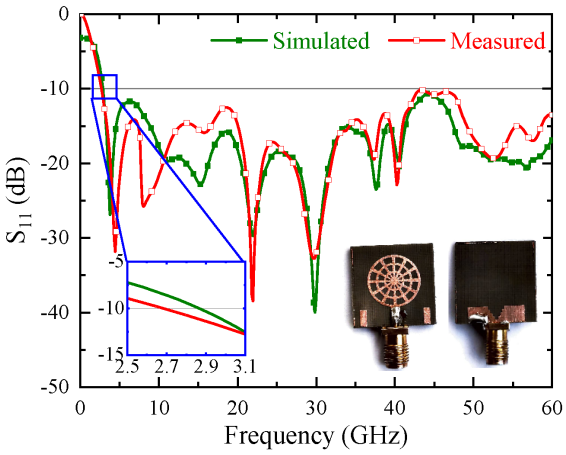

Figure 5. Simulated and measured S_{11} response of the proposed antenna.

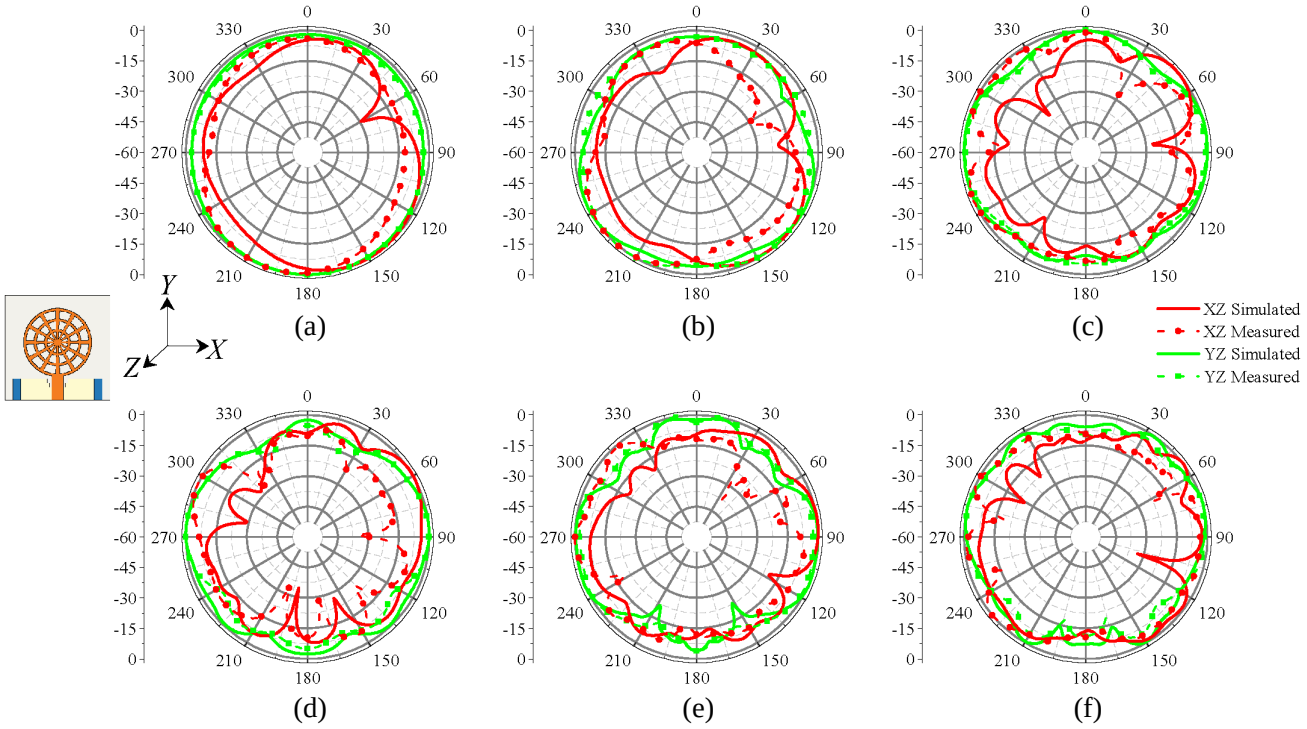

Figure 6. Simulated and measured normalized radiation patterns of the proposed antenna at (a) 5 GHz, (b) 15 GHz, (c) 25 GHz, (d) 35 GHz, (e) 45 GHz, (f) 55 GHz.

Power Network Analyzer (PNA). Figure 5 illustrates a comparison between the simulated and measured S_{11}, and they are found to be in fair agreement. According to the measured results, the antenna can operate in the frequency range of 2.70–60 GHz. A slight mismatch is observed between the results, which might be accounted for by imperfect SMA connector soldering, fabrication tolerances, and scattering environmental losses.

In Figure 6, the simulated and measured radiation characteristics for the YZ- and XZ-planes are shown. Radiation patterns are observed at six different frequencies to cover the entire operating range. Radiation characteristics are demonstrated to be omnidirectional in both planes for lower frequency bands, as shown in Figures 6(a), (b). However, for higher frequencies (Figures 6(c)–(f)), the antenna exhibits omnidirectional patterns with some distortions in both planes, which is attributed to the

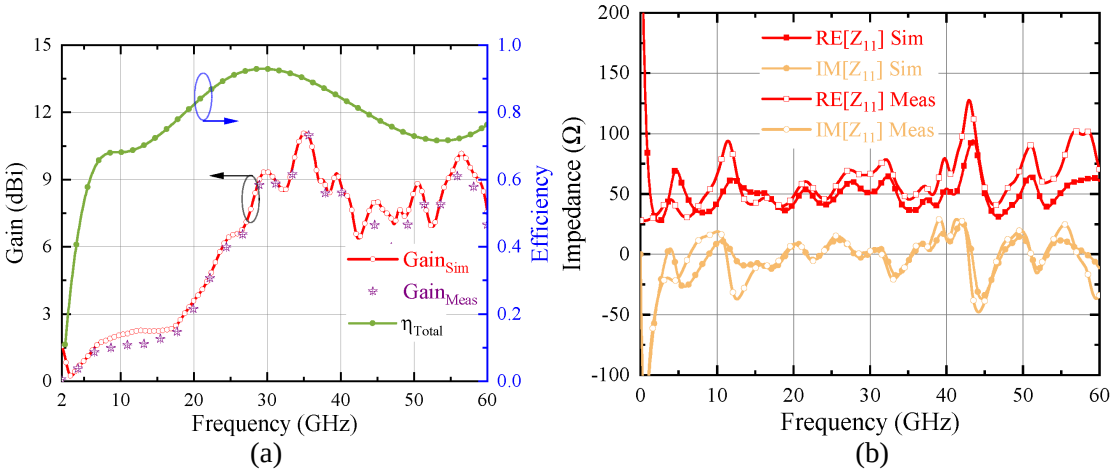

Figure 7. Experimental results of the proposed antenna: (a) gain and efficiency; (b) real and imaginary parts of the input impedance.

excitation of higher-order modes [13].

In Figure 7(a), simulated and measured gains vs. frequency curves are illustrated. It is noted that the maximum gain value is ≈ 11 dBi for simulation, while the experimental peak gain value is ≈ 10.3 dBi. One thing can be observed from the gain curve: it increases with the increase in frequency up to 34 GHz. For frequencies beyond 34 GHz, the gain decreases. This happens due to high dielectric losses at higher frequencies. Furthermore, the electrical dimensions of the radiating element become large, and due to inverse currents, anti-resonance is excited, which results in a low gain [6]. The simulated total efficiency (η_{Total}) results are also shown in Figure 7(a). For SWB antennas, efficiency is one of the key parameters defining the radiation capabilities of the antenna. As shown in the figure, the proposed antenna has a high value of efficiency within the operating range, establishing it as a potential candidate for SWB operation.

Moving next, the simulated and measured input impedance results of the proposed antenna are shown in Figure 7(b). It can be concluded from the figure that the resistance (real part) and reactance (imaginary part) of the antenna's impedance fluctuate around 50 Ω and 0 Ω, respectively, maintaining the overall impedance $\sim 50\,\Omega$ within the operating range. The low-dispersive behavior of the proposed antenna for both the near- and far-field behaviors is a very important feature, typically offered by antennas based on the self-similarity principle [23]. According to this, such an antenna always behaves in the same way (from the radiation and impedance points of view) because the active zone responsible for radiation is identical, compared to the wavelength, in all the frequency ranges, but these antennas suffer from large footprint [24]. The antenna design presented in this work maintains almost constant radiation patterns and impedance response throughout the frequency band, despite its compact layout. As a comparison, an Archimedean spiral operating at 2 GHz should have a radius greater than 20 mm [24].

As a consequence, the proposed antenna could play a strategic role in future sixth-generation (6G) architectures, where small, widespread electronic devices will have to be autonomous from an energy point of view. An almost omnidirectional antenna with almost constant input impedance is extremely useful as an SWB rectenna (rectifying antenna) for energy harvesting applications, especially when the direction of the incoming signal is unknown, and the frequency of the incoming signal can fall in the SWB range. Moreover, the matching network between the antenna and the nonlinear rectifying section can be straightforward thanks to the almost constant input impedance offered by the proposed antenna. However, designing the matching network is out of the scope of the presented work, and this will be part of a future research activity.

A comparative study is conducted between the proposed work and earlier reported SWB antennas, and the results are listed in Table 2. Results confirmed that the proposed antenna is miniaturized by 4.30% compared to the smallest prototype and provides a wider operating bandwidth than other designs. The proposed design also offers better RBW and FBW than [7–11, 16–18] with higher BDR

Table 2. Comparison between previously presented and proposed SWB antennas.

Ref.	Size $(L \times W)$ mm^2	Size $(\lambda_l \times \lambda_w)$ mm^2	Operating BW (GHz)	RBW	FBW	Peak Gain (dBi)	BDR	% Size reduction compared to the proposed design
[3]	150×156	0.21×0.20	0.4–16	40 : 1	190.2	6	4515	98.29
[4]	150×150	0.36×0.36	0.72–25	34.72 : 1	188.8	7	1457	98.22
[5]	124×110	0.37×0.42	1.02–24.1	23.63 : 1	183.7	7	1167	97.07
[6]	124×120	0.43×0.44	1.08–27.40	25 : 1	184.8	6.2	959	97.31
[7]	35×77	0.17×0.37	1.44–18.8	13.05 : 1	172	7	2735	85.16
[8]	38×55	0.55×0.38	3–35	11.66 : 1	168	4	805	80.86
[9]	30×40	0.30×0.23	2.26–22.18	9.81 : 1	163	6.5	2393.7	66.67
[10]	45×30	0.47×0.31	3.15–32	10.16 : 1	164.1	4.8	1126.6	70.37
[11]	52.25×42	0.22×0.18	1.3–20	15.38 : 1	175.6	4.18	4261	81.77
[14]	170×150	0.325×0.368	0.65–35.61	54.78 : 1	193	6.5	1613.7	98.43
[15]	28×19	0.29×0.17	0.7–18.5	26.42 : 1	185.41	6.1	38849	24.81
[16]	35×30	0.326×0.28	2.8–40	14.28 : 1	173.8	6.1	1904	61.90
[17]	22×19	0.27×0.23	3.7–60	16.21 : 1	176.76	6.2	2780	4.30
[18]	47.5×35.1	0.21×0.285	1.8–30	16.9 : 1	178	5	3062	76.00
Proposed	20×20	0.19×0.19	2.86–60	21 : 1	181.8	≈ 11	5036	–

than all designs except [15]. Furthermore, the proposed design offers a high peak gain compared to the designs listed in Table 2.

4. TIME DOMAIN ANALYSIS

Time domain analysis is necessary to assess the antenna's performance over a super-wide frequency band while transmitting or receiving pulse signals [23]. For time-domain analysis, two identical antennas operating in transceiver mode, separated by 10 cm, are placed in face-to-face (F2F) and side-by-side (SbS) configurations, respectively, as shown in Figures 8(a) and 8(b).

To excite the antennas, a Gaussian pulse centered at 30.5 GHz with a frequency band of 1–60 GHz is utilized. The normalized amplitudes of both input and output signals for both configurations are shown in Figure 9. The cross-correlation between transmitted and received signals is calculated using Equation (1) and is known as the fidelity factor (FF) [25].

$$\mathrm{FF} = \max \left[\frac{\int_{-\infty}^{\infty} S_t(t) S_r(t+\tau) d\tau}{\int_{-\infty}^{\infty} |S_t(t)|^2 dt \int_{-\infty}^{\infty} |S_r(t)|^2 dt} \right]. \tag{1}$$

In Equation (1), $S_t(t)$ and $S_r(t)$ indicate transmitted and received signals, respectively, and τ represents the group delay. The FF values for F2F and SbS configurations are 79% and 85%, respectively. As can be seen, the FF is higher for SbS configuration, which means that the transmitted signal will be less distorted than F2F configuration.

Group delay, $\tau_g(\omega)$, quantifies the transition time taken by the signal to travel through a device and is defined as the negative rate of change of the transfer function phase, $\phi(\omega)$, with respect to frequency [23]. Mathematically, $\tau_g(\omega)$ can be calculated as

$$\tau_g(\omega) = -\frac{d\phi(\omega)}{d\omega} = -\frac{d\phi(\omega)}{2\pi df}. \tag{2}$$

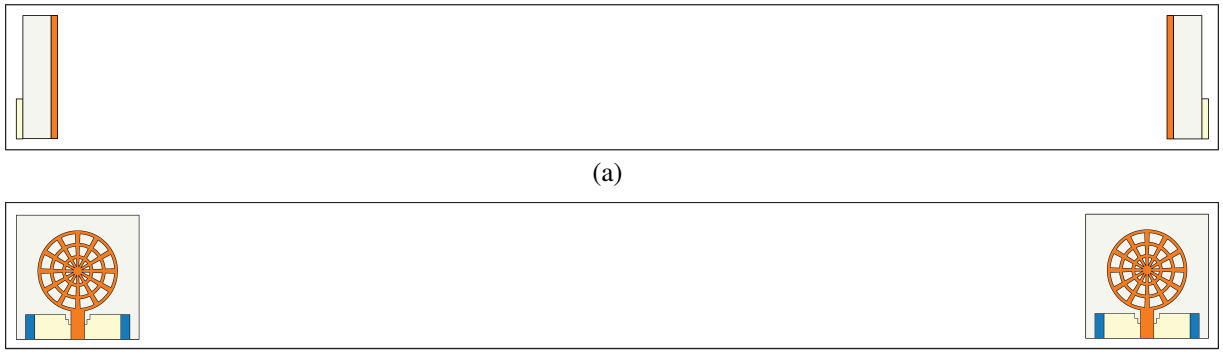

Figure 8. Time domain analysis of the proposed antenna. (a) F2F configuration. (b) SbS configuration.

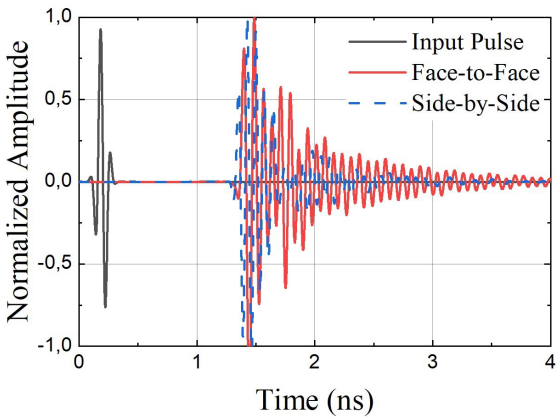

Figure 9. Pulse response of the proposed antenna in the time domain.

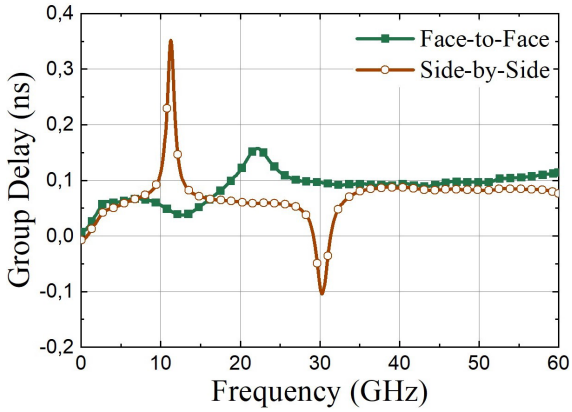

Figure 10. Group delay profile of the proposed antenna for F2F and SbS configurations.

The simulated $\tau_g(\omega)$ response is plotted in Figure 10 for both configurations. For UWB applications, $|\tau_g| \leq 1$ ns is desirable to ensure linearity of phase in the far field region. From Figure 10, it is observed that the $|\tau_g|$ value is within 0.5 ns for the entire frequency range [26].

5. CONCLUSION

In this work, a compact SWB planar fractal antenna is reported for microwave and mmWave applications. The radiator geometry consists of three annular rings connected through conical-shaped metallic strips. Furthermore, the proposed antenna has a stair-type defect in the partial ground plane designed at the bottom of the substrate. To reduce the lower frequency limit, two rectangular parasitic strips are inserted at the top of the substrate. The proposed design has an IBW of 57.14 GHz from 2.86 to 60 GHz. The antenna also offers an RBW of 21 : 1 and an FBW of 181.8%, still guaranteeing almost unchanged performance from both the near- and far-field points of view. Furthermore, the BDR of the antenna is fairly large, which signifies its compactness. The proposed antenna is fabricated and measured, and it is observed that the two results are in good agreement. The gain of the proposed design varies from 2 to 11 dBi, with an average gain of $\approx$ 6 dBi over the entire frequency range. It can be demonstrated that the proposed antenna can be utilized in many applications such as wireless communication, radar communications, satellite and defense communication, radio determination, Doppler navigation aids, radio astronomy, aeronautical radio navigation, and very-small-aperture terminal (VSAT)/satellite news gathering (SNG) applications. In addition, the proposed antenna can play a strategic role in future rectennas for 5G and 6G networks, where pervasively distributed devices must be autonomous from an energy point of view.

REFERENCES

1. Liang, X. L., S. S. Zhong, and W. Wang, "Elliptical planar monopole antenna with extremely wide bandwidth," *Electronics Letters*, Vol. 42, No. 8, 441–442, 2006.
2. Yan, X. R., S. S. Zhong, and X. L. Liang, "Compact printed semi-elliptical monopole antenna for super-wideband applications," *Microwave and Optical Technology Letters*, Vol. 49, No. 9, 2061–2063, 2007.
3. Dong, Y., W. Hong, L. Liu, Y. Zhang, and Z. Kuai, "Performance analysis of a printed super-wideband antenna," *Microwave and Optical Technology Letters*, Vol. 51, No. 4, 949–956, 2009.
4. Liu, J., K. P. Esselle, S. G. Hay, and S.-S. Zhong, "Study of an extremely wideband monopole antenna with triple band-notched charactersistics," *Progress In Electromagnetics Research*, Vol. 123, 143–158, 2011.
5. Liu, J., S. Zhong, and K. P. Esselle, "A printed elliptical monopole antenna with modified feeding structure for bandwidth enhancement," *IEEE Transactions on Antennas and Propagation*, Vol. 59, No. 2, 667–670, 2010.
6. Liu, J., K. P. Esselle, S. G. Hay, and S. Zhong, "Achieving ratio bandwidth of 25 : 1 from a printed antenna using a tapered semi-ring feed," *IEEE Antennas and Wireless Propagation Letters*, Vol. 10, 1333–1336, 2011.
7. Chen, K. R., J. S. Row, et al., "A compact monopole antenna for super wideband applications," *IEEE Antennas and Wireless Propagation Letters*, Vol. 10, 488–491, 2011.
8. Gorai, A., A. Karmakar, M. Pal, and R. Ghatak, "A CPW-fed propeller shaped monopole antenna with super wideband characteristics," *Progress In Electromagnetics Research C*, Vol. 45, 125–135, 2013.
9. Tang, M. C., R. W. Ziolkowski, and S. Xiao, "Compact hyper-band printed slot antenna with stable radiation properties," *IEEE Transactions on Antennas and Propagation*, Vol. 62, No. 6, 2962–2969, 2014.
10. Hakimi, S., S. K. A. Rahim, M. Abedian, S. Noghabaei, and M. Khalily, "CPW-fed transparent antenna for extended ultrawideband applications," *IEEE Antennas and Wireless Propagation Letters*, Vol. 13, 1251–1254, 2014.
11. Samsuzzaman, M. and M. T. Islam, "A semicircular shaped super wideband patch antenna with high bandwidth dimension ratio," *Microwave and Optical Technology Letters*, Vol. 57, No. 2, 445–452, 2015.
12. Rafique, U., M. M. Ahmed, M. M. Hassan, and H. Khalil, "A modified super-wideband planar elliptical monopole antenna," *2018 Progress In Electromagnetics Research Symposium (PIERS-Toyama)*, 2344–2349, Toyama, Japan, Aug. 1–4, 2018.
13. Rafique, U. and S. U. Din, "Beveled-shaped super-wideband planar antenna," *Turkish Journal of Electrical Engineering and Computer Science*, Vol. 26, No. 5, 2417–2425, 2018.
14. Singhal, S. and A. K. Singh, "Elliptical monopole based super wideband fractal antenna," *Microwave and Optical Technology Letters*, Vol. 62, No. 3, 1324–1328, 2020.
15. Ramanujam, P., P. G. R. Venkatesan, C. Arumugam, and M. Ponnusamy, "Design of miniaturized super wideband printed monopole antenna operating from 0.7 to 18.5 GHz," *International Journal of Electronics and Communications*, Vol. 123, 153273, 2020.
16. Kundu, S. and A. Chatterjee, "A compact super wideband antenna with stable and improved radiation using super wideband frequency selective surface," *International Journal of Electronics and Communications*, Vol. 150, 154200, 2020.
17. Gaur, S., D. Lohdi, S. Singhal, and M. Salim, "Compact flower shape super wideband antenna for mmWave applications," *URSI-RCRS*, 1–4, 2022.
18. Lazovic, L., B. Jokanovic, V. Rubezic, M. Radovanovic, and A. Jovanovic, "Fractal cardioid slot antenna for super wideband applications," *Electronics*, Vol. 11, 1043, 2020.
19. Balanis, C. A., *Antenna Theory: Analysis and Design*, John Wiley & Sons, 2016.

20. Ray, K. P., "Design aspects of printed monopole antennas for ultra-wide band applications," *International Journal of Antennas and Propagation*, 2008.
21. Ray, K. and Y. Ranga, "Ultra-wideband printed modified triangular monopole antenna," *Electronics Letters*, Vol. 42, No. 19, 1, 2006.
22. Ray, K. P. and Y. Ranga, "Ultrawideband printed elliptical monopole antennas," *IEEE Transactions on Antennas and Propagation*, Vol. 55, No. 4, 1189–1192, 2007.
23. Wiesbeck, W., G. Adamiuk, and C. Sturm, "Basic properties and design principles of UWB antennas," *Proceedings of the IEEE*, Vol. 97, No. 2, 372–385, 2009.
24. Agarwal, S., D. Masotti, S. Nikolaou, and A. Costanzo, "Conformal design of a high-performance antenna for energy-autonomous UWB communication," *Sensors*, Vol. 21, No. 17, 5939, 2021.
25. Singhal, S. and A. K. Singh, "CPW-fed hexagonal Sierpinski super wideband fractal antenna," *IET Microwaves, Antennas & Propagation*, Vol. 10, No. 15, 1701–1707, 2016.
26. Kwon, D. H., "Effect of antenna gain and group delay variations on pulse-preserving capabilities of ultrawideband antennas," *IEEE Transactions on Antennas and Propagation*, Vol. 54, No. 8, 2208–2215, 2006.